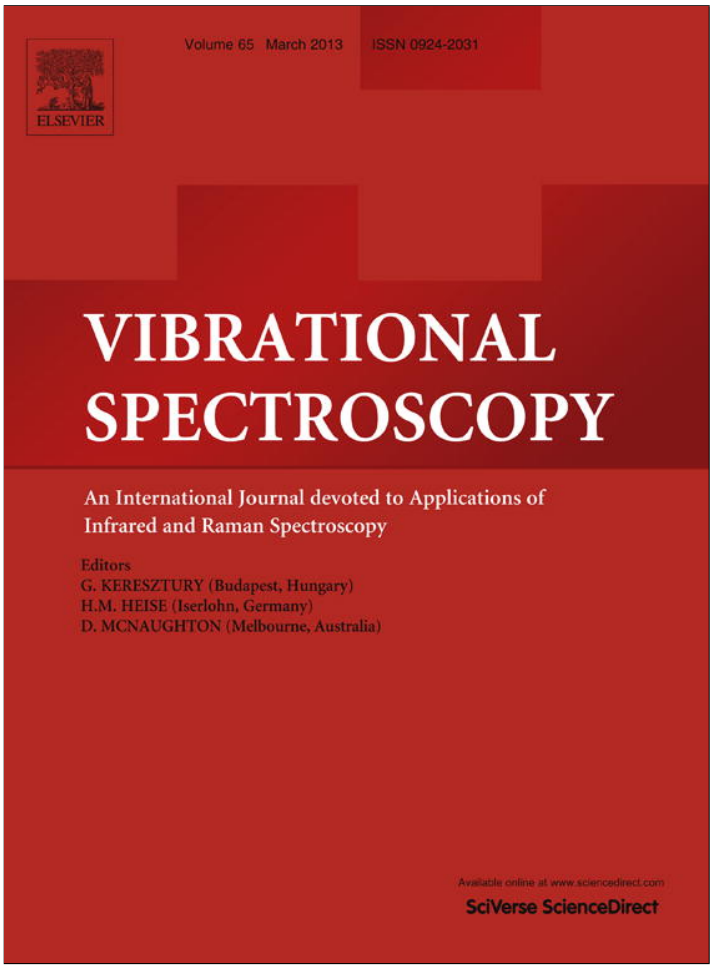

Vibrational Spectroscopy 65 (2013) 124–131

Contents lists available at SciVerse ScienceDirect

Vibrational Spectroscopy

journal homepage: www.elsevier.com/locate/vibspec

Trimethylsilyl trichloroacetate vibrational, structural and electronic properties and their comparison with related acetates

M.E. Defonsi Lestard, R.A. Cobos Picot, M.E. Tuttolomondo, A. Ben Altabef*,[1]

INQUINOA-CONICET, Instituto de Química Física, Facultad de Bioquímica, Química y Farmacia, Universidad Nacional de Tucumán, San Lorenzo 456, T4000CAN S.M. de Tucumán, Argentina

ARTICLE INFO

Article history:
Received 6 June 2012
Received in revised form
23 November 2012
Accepted 23 November 2012
Available online 22 December 2012

Keywords:
Ab initio calculations
DFT calculations
Natural bond orbital analysis
Infrared spectroscopy
Raman spectroscopy
Trimethylsilyl trichloroacetate

ABSTRACT

The molecular structure of trimethylsilyl trichloroacetate, $CCl_3C(O)OSi(CH_3)_3$, was determined by ab initio (MP2) and DFT calculations using 6-31G(d), 6-311G(d,p), 6-311++G(d,p) and 6-311++G(3df,3pd) basis sets. The infrared and Raman spectra for the liquid phase were also recorded and the bands observed assigned to the vibrational normal modes. The study was completed using natural bond orbital (NBO) analysis and atoms in molecules (AIM) calculations. The comparison between the calculated molecular geometrical parameters, conformation and vibrational properties and those measured for $CX_3C(O)OR$ [X = F, Cl and R = CH_3, $Si(CH_3)_3$] was of particular interest in order to check the behavior of the C═O and C—O with respect to the different substitutions. The experimental vibrational data, along with calculated theoretical force constants, were used to define a scaled quantum mechanical force field for the target system that enabled us to estimate the measured wavenumbers with a final root-mean-square deviation of 8.92 cm^{-1}.

1. Introduction

Trimethylsilyl trichloroacetate is a convenient reagent for the silylation of phenols, carboxylic acids, mercaptans, amides, acetylenes, and β-keto esters, while the reaction with aldehydes and ketones creates silylated trichloromethyl carbinols [1–11].

Trimethylsilyl trichloroacetate is a commercially available substance whose molecular structure and vibrational characteristics are still not known. Therefore, it was decided to extend our previous studies on different derivatives of acetic acid [12–15] to this substance in order to have more information about the conformation and force constants of this kind of molecules. For that purpose, the barriers to internal rotation for both the CCOSi and COSiC dihedral angles were calculated using the RHF, MP2 and B3LYP methods with the 6-311++G(d,p) basis set.

The infrared and Raman spectra were measured for the substance and the molecular structure and vibrational wavenumbers were calculated by means of quantum chemistry procedures. The spectral features were subsequently assigned to the different normal modes of vibration and a set of force constants in the form of a scaled quantum mechanic (SQM) force field was obtained. The study was completed using natural bond orbital (NBO) analysis and atoms in molecules (AIM) calculations.

The comparison between the calculated molecular geometrical parameters, conformation and vibrational properties and those measured for $CX_3C(O)OR$ [X = F, Cl and R = CH_3, $Si(CH_3)_3$] [13,14,16] was of particular interest in order to check the behavior of the C═O and C—O with respect to the different substitutions. When R is more electropositive there is an increase in the interaction of lone pairs (LP) from O to the σ^* C═O, with an increase in electron delocalization of the O—C═O group. The lone pairs of Cl and F atoms and their interaction on the σ^* C—C and σ^* C═O play an important role in the strength of these bonds.

2. Materials and methods

Trimethylsilyl trichloroacetate, $CCl_3C(O)OSi(CH_3)_3$ is a commercially available substance, purum, ≥98%(GC) (Sigma–Aldrich Products, Inc.), was used with no further purification and was handled with proper protection from the atmospheric humidity.

The infrared spectrum of trimethylsilyl trichloroacetate in the liquid phase was recorded in the 4000–400 cm^{-1} range using a Perkin-Elmer GX1 FTIR instrument. KBr windows were used to record the infrared spectra of liquid substance. The resolution of

* Corresponding author. Tel.: +54 381 4311044; fax: +54 381 4248169.
E-mail address: altabef@fbqf.unt.edu.ar (A. Ben Altabef).
[1] Member of the Carrera del Investigador Científico, CONICET, Argentina.

0924-2031/$ – see front matter © 2012 Elsevier B.V. All rights reserved.
http://dx.doi.org/10.1016/j.vibspec.2012.11.014

the equipment employed was 1 cm^{-1}. A total of 32 scans were done in each condition and the spectra were analyzed using the OMNIC v.7.2 mathematical software provided by the manufacturer. The polarized Raman spectra of the liquid at room temperature, polarized at 0 and 90°, were obtained with a Perkin-Elmer FT-Raman RFS 100/S spectrometer using 1064 nm light from an Nd/YAG laser for excitation (spectral resolution 4 cm^{-1}). The liquid sample was handled in flame-sealed capillaries (4 mm o.d.).

3. Computational methods

Calculations were performed with the Gaussian 03 suite of programs [17]. Geometry optimizations were performed at the MP2 [18] and DFT levels using a variety of basis sets. Electron correlation was then considered by means of the MP2 approach with the 6-311++G(d,p), 6-311++G(3df,3pd) and 6-311G(d,p) basis sets [19–22]. DFT calculations were performed with Becke's three-parameter hybrid exchange functional [23] (B3) combined with both the Lee–Yang–Parr gradient-corrected correlation functional [24] (LYP) and the same basis sets used for the MP2 calculations. All calculations were performed with standard gradient techniques and default convergence criteria. Stationary points were assessed with analytical second derivatives of the energies, with zero-point energy corrections neglected. The potential energies associated with the CCOSi dihedral angle were calculated at RHF, MP2, B3LYP and mPW1PW91 [25] levels using the 6-311++G(d,p) basis set, with that torsional angle frozen and all other parameters allowed to relax. The total energy curve was constructed in steps of 5 or 10° using default convergence criteria as implemented in the Gaussian programs [17].

A natural bond orbital (NBO) calculation was performed at the RHF/6-311++G(d,p) level with the NBO 3.1 program [26] as implemented in the Gaussian 03 package.

Besides, an analysis of the reactivity of trimethylsilyl trichloroacetate was done within Bader's atoms in molecules theory (AIM) by using AIM2000 code [27,28].

The calculation of force constants for trimethylsilyl trichloroacetate included force-field transformation, scaling and determination of the potential-energy distribution, all of which were performed using the FCARTP program [29]. The atomic displacements given by the Gaussian 03 program for each vibrational mode were used to understand the nature of the molecular vibrations qualitatively and, for that purpose, the corresponding data were represented graphically using the GaussView program [30].

3.1. Prediction of Raman intensities

The Raman activities (SRa) were calculated with the Gaussian 03 program converted to relative Raman intensities (IRa) using the following relationship derived from the intensity theory of Raman scattering [31]:

$$I_i = \frac{f(\nu_0 - \nu_i)^4 S_i}{\nu_i[1 - \exp(hc\nu_i/k_bT)]} \quad (1)$$

where ν_0 is the laser exciting wavenumber in cm^{-1} (in this work, we have used the excitation wavenumber ν_0 = 9398.5 cm^{-1}, which corresponds to the wavelength of 1064 nm of a Nd:YAG laser), ν_i the vibrational wavenumber of the ith normal mode (cm^{-1}), while S_i is the Raman scattering activity of the normal mode ν_i. f (a constant equal to 10^{-12}) is a suitably chosen common normalization factor for all peak intensities.

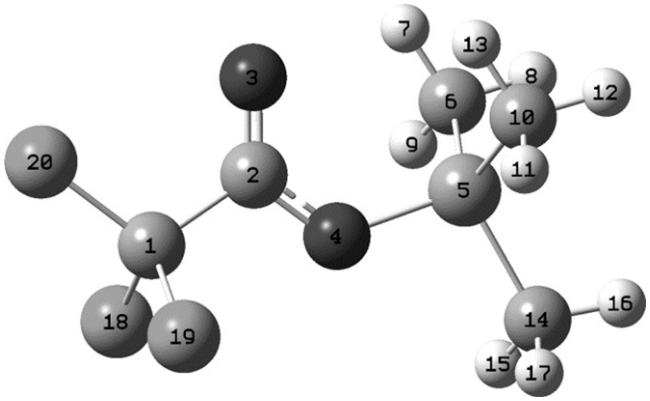

Fig. 1. Molecular structures (including atom numbering) of $CCl_3C(O)OSi(CH_3)_3$.

4. Results and discussion

4.1. Quantum chemical calculations

All geometry optimizations (RHF, MP2 and DFT with all basis sets) predicted a strong preference (36.9 kJ mol^{-1}) for the staggered *anti* conformation, as shown in Fig. 1.

In order to understand the significance of the results, the conformational potential energy barrier was studied according to the variation of the CCOSi and COSiC torsion angles, which was calculated with B3LYP/6-311G(d,p). Fig. 2(a) shows the variation of the CCOSi dihedral angle, where the change of substituents in different sizes and electronegativity (Cl, F) gives as a result a lower torsion barrier for the chlorinated compound while the substituent change does not affect the COSiC angle of the torsion barrier (Fig. 2(b)).

Based on these results and using the concept of "conformational transfer", we employed the trimethylsilyl trifluoroacetate experimental electron-diffraction structure [14] for a comparison with the trimethylsilyl trichloroacetate (Table 1) calculated values.

Inclusion of extra polarization functions (beyond a single d function) was necessary to predict the bond lengths accurately as previously found for the $CF_3C(O)OSi(CH_3)_3$ [14] related molecule [12,13,15]. The root-mean-square deviations (RMSD) of the various calculations from the experimental values for $CF_3C(O)OSi(CH_3)_3$ are also shown in Table 1.

There is a lengthening of the distance C—C(O) and O—Si as seen from the comparison of the distances calculated by different methods for the replacement of the F atom by the Cl atom. With regard to the angles, there is an increase in the C—C=O and C—C—O angles and a decrease in the O=C—O angle, where F is replaced by Cl.

4.2. Vibrational analysis

The assignment of the experimental bands to the normal modes of vibration of $CCl_3C(O)OSi(CH_3)_3$ was based on comparison with data for related molecules and on the results of the calculations [B3LYP/6-311++G(d,p)]. Representative spectra are illustrated in Fig. 3 (infrared spectra of the liquid and scaled), Fig. 4 (polarized Raman spectra of the liquid) and Fig. 5 (Raman spectra of the liquid and simulated Raman spectra using Raman intensities according to formula (1)).

The B3LYP calculation reproduced the normal wavenumbers for $CCl_3C(O)OSi(CH_3)_3$ with root-mean-square deviations (RMSD) of 62 cm^{-1} for the 6-31G(d) basis set, 59.6 cm^{-1} for 6-311G(d,p) and 62.44 cm^{-1} for 6-311++G(d,p). The results with the combination B3LYP/6-311++G(d,p) were used for the vibrational analysis to facilitate the comparison of the present results with those obtained previously for related molecules. The wavenumbers calculated

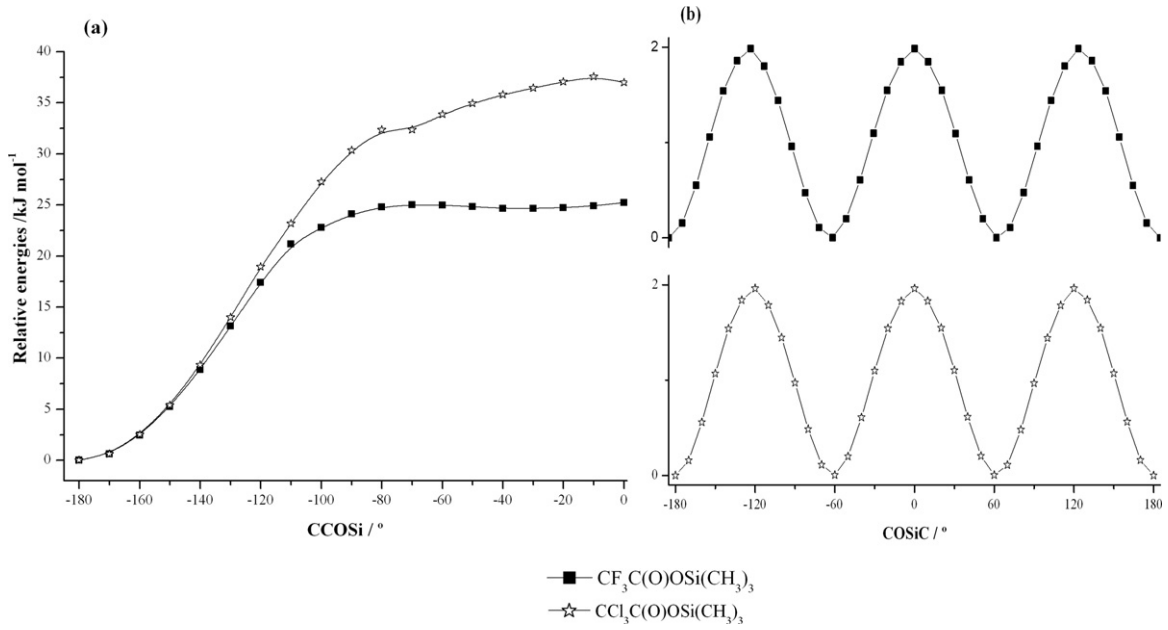

Fig. 2. Torsional potentials about (a) the CCOSi dihedral angle for the and (b) the COSiC dihedral angle of $CCl_3C(O)OSi(CH_3)_3$ and $CF_3C(O)OSi(CH_3)_3$ calculated at B3LYP/6-311++G(d,p).

Table 1
Geometrical parameters for $CCl_3C(O)OSi(CH_3)_3$ at different levels of theory and compared with the $CF_3C(O)OSi(CH_3)_3$ experimental and theoretical parameters.[a]

	GED[a]	$CF_3C(O)OSi(CH_3)_3$			$CCl_3C(O)OSi(CH_3)_3$		
		MP2[a]	B3LYP[a]		MP2	B3LYP	
		6-311G(d,p)	6-311g++(3df,3pd)	6-311++G(d,p)	6-311G(d,p)	6-311g++(3df,3pd)	6-311++G(d,p)
Distances (pm)[a]							
C(1)—F(2)	131.7	132.9	132.8	133.4	176.0	176.7	177.8
C(1)—F(3.4)	133.9	133.9	134.2	134.8	177.6	179.0	180.1
C(1)—C(19)	155.6	153.9	155.4	155.4	155.0	156.2	156.4
C(19)═O(20)	119.5	120.8	119.8	120.1	121.7	120.0	120.1
C(19)—O(18)	130.7	132.6	131.6	131.7	133.0	131.6	131.7
O(18)—Si(17)	171.9	173.6	173.0	175.2	175.2	172.6	174.7
Si(17)—C(5.6)	185.7	186.2	186.4	187.0	186.6	186.4	187.1
Si(17)—C(7)	185.9	186.0	186.3	186.8	186.8	186.3	186.9
RMSD (pm)		1.6	0.5	2.2			
Angles (°)							
F—C(1)—C(19)	110.3	110.5	110.7	110.8	110.0	110.7	110.5
C(1)—C(19)═O(20)	122.2	122.7	121.9	121.9	122.9	122.2	122.3
C(1)—C(19)—O(18)	108.4	110.0	110.5	110.4	110.5	111.2	110.9
C(19)—O(18)—Si(17)	124.0	122.3	125.9	125.9	120.8	125.8	126.0
O(18)—Si(17)—C(7)	102.4	102.2	102.1	101.8	101.4	102.0	101.8
O(18)—Si(17)—C(5.6)	108.1	108.4	108.2	107.8	108.3	108.4	107.9
RMSD (°)		1.0	1.4	1.4			

[a] Ref. [14].

with this method for the 54 modes of vibration (32 A′ and 22 A″) of $CCl_3C(O)OSi(CH_3)_3$ appear in Table 2, where they are compared with the measured values.

The polarized Raman spectra at 0° and 90° with respect to the plane of polarization of the exciting light also served to confirm some assignments. The theoretical coefficients of depolarization are $0 \leq \rho s < 3/4$ for the A′ modes and $\rho s = 3/4$ for the A″ modes (Fig. 4).

4.2.1. Methyl group modes

Two clearly defined bands and some shoulders appear in the infrared and Raman spectra of the liquid substance in the 3000–2900 cm^{-1} region, which can be assigned to the expected nine CH_3 stretching modes.

The bands located at 2960 and 2902 cm^{-1} and a shoulder at 2965 cm^{-1} were observed in the infrared spectrum for the nine CH_3 stretching modes corresponding to the antisymmetric and symmetric stretchings, respectively.

The comparison between $CF_3C(O)OSi(CH_3)_3$ [14] and $CF_3SO_2OSi(CH_3)_3$ [32] shows that the 2965 cm^{-1} band should be associated with the CH_3 group antisymmetric stretching. The bands observed at 1414 cm^{-1} and 1384 cm^{-1} in the Raman spectrum were assigned to the six antisymmetric CH_3 deformation modes. The other CH_3 symmetric modes were assigned to the band at 1309 and 1272 cm^{-1}. These results agree with the ordering predicted by the B3LYP calculation and bands observed for related molecules with $Si(CH_3)_3$ groups [14,32]. The six rocking modes of the CH_3 group were located at 858, 773, 766 and 705 cm^{-1}.

4.2.2. Trimethylsilyl group modes

The $Si(CH_3)_3$ antisymmetric stretching modes were assigned to the weak bands at 703 and 698 cm^{-1} in the Raman spectrum of

Table 2
Observed and calculated wavenumbers, infrared and Raman intensities and potential-energy distribution for $CCl_3C(O)OSi(CH_3)_3$.

Mode	Infrared[a] (liquid)	Raman[a] (liquid)	Calculated[a]	Calculated SQM[b]	IR intensity[c]	Raman intensity[d]	Potential-energy distribution[e]	Approximate description of mode
A′								
1	2965 sh	2965 (34)	3113	2979	5.29	53.34	46 S_1 + 44 S_{33}	ν_a CH_3
2	2965 sh	2965(34)	3106	2964	7.56	25.14	100 S_2	ν_a CH_3
3	2965 sh	2965 (34)	3098	2959	18.00	71.78	45 S_3 + 43 S_{35}	ν_a CH_3
4	2902 w	2906 (100)	3029	2898	5.28	105.0	54 S_4 + 22 S_5 + 22 S_6	ν_s CH_3
5	2902 w	2906 (100)	3027	2896	1.35	100.7	45 S_4 + 27 S_5 + 15 S_6	ν_s CH_3
6	2902 w	2906 (100)	3026	2896	3.28	100.0	49 S_5 + 46 S_6	ν_s CH_3
7	1752 s	1752 (11)	1798	1752	230.00	9.21	99 S_7	ν C=O
8	1384 w	1384 (6)	1477	1418	16.50	0.60	35 S_8 + 35 S_9 + 22 S_{12}	δ_a CH_3
9	1384 w	1384 (6)	1465	1407	3.55	0.11	19 S_8 + 19 S_9 + 13 S_{36}	δ_a CH_3
10	1384 w	1384 (6)	1462	1399	9.39	5.70	12 S_8 + 12 S_{36} + 71 S_{10}	δ_a CH_3
11	1309 w	1311 (9)	1312	1269	30.55	2.15	35 S_{11} + 35 S_{12} + 45 S_{18}	δ_s CH_3
12	1272 w	1270 (10)	1304	1261	51.20	0.50	54 S_{12} + 12 S_{11}	δ_s CH_3
13	1272 w	1270 (10)	1302	1253	48.34	0.02	30 S_{39} + 30 S_{13}	δ_s CH_3
14	1259 s	1260 (10)	1276	1252	534.27	2.37	50 S_{14} + 51 S_{39}	ν C(16)—O(28)
15	970 m	970 (3)	966	968	82.85	0.73	74 S_{15} + 16 S_{24}	ν C(21)—C(28)
16	848 vs	858 (9)	889	862	111.46	0.28	12 S_{16} + 12 S_{22}	ρ CH_3
17	832 m	832 (10)	830	832	164.01	5.93	56 S_{17} + 14 S_{26}	ν_a CCl_3
18	772 sh	773 (8)	794	774	46.00	2.65	23 S_{15} + 15 S_{18} + 10 S_{24}	ρ CH_3
19	759 d	766 sh	784	757	46.17	0.92	12 S_{17} + 15 S_{19} + 12S_{43}	ρ CH_3
20	735 w	733 (14)	737	729	73.00	3.07	27 S_{20} + 20 S_{21}	δ in-of-plane C=O
21	698 sh	697 (17)	708	686	12.59	0.10	36 S_{21} + 34 S_{39}	ν_{as} Si—C
22	679 m	688 (17)	686	670	40.25	3.27	38 S_{19} + 40 S_{22}	ν Si—O
23	621 w	616 (80)	600	600	2.67	18.2	88 S_{23}	ν_s Si—C
24	436 w	436 (97)	425	422	1.06	11.87	10 S_{15} + 63 S_{24}	ν_s CCl_3
25	–	377 (3)	370	375	7.00	5.86	23 S_{25} + 47 S_{44}	δ_s CCl_3
26	–	321 (31)	303	305	5.25	1.00	17 S_{25} + 30 S_{26} + 29 S_{27}	δ_{as} CCl_3
27	–	275 (44)	270	270	20.15	2.56	51 S_{27} + 49 S_{28}	δ_s Si—C
28	–	258 (40)	269	260	3.88	5.24	17 S_{26} + 36 S_{28} + 10 S_{29}	δ_{as} Si—C
29	–	258 (40)	252	212	3.78	0.15	20 S_{26} + 45 S_{28} + 39 S_{29}	δ Si—O—C
30	–	214 sh	211	160	1.99	0.61	24 S_{28} + 15 S_{30}	ρ Si—C
31	–	168 (50)	147	143	0.86	1.55	32 S_{31} + 26 S_{28} + 21 S_{32}	ρ CCl_3
32	–	–	72	–	0.53	0.00	–	δ C—C—O
A″								
33	2960 w	2960 sh	3112	2978	1.70	25.04	44 S_1 + 46 S_{33}	ν_{as} CH_3
34	2960 w	2960 sh	3094	2972	6.74	67.90	88 S_{34}	ν_{as} CH_3
35	2960 w	2960 sh	3094	2960	2.43	29.50	11 S_{34} + 40 S_3 + 40 S_{35}	ν_{as} CH_3
36	1414 w	1414 (12)	1459	1404	1.35	21.34	46 S_{36} + 46 S_{37}	δ_{as} CH_3
37	1414 w	1414 (12)	1457	1401	0.33	13.88	34 S_{36} + 34 S_{37} + 30 S_{38}	δ_{as} CH_3
38	1414 w	1414 (12)	1450	1392	0.04	0.57	29 S_8 + 29 S_9 + 33 S_{38}	δ_{as} CH_3
39	848 vs	858 (9)	886	852	101.20	0.58	12 S_{16} + 12 S_{17} + 13 S_{39} + 13 S_{40}	ρ CH_3
40	848 vs	858 (9)	881	842	203.60	0.47	56 S_{40} + 15 S_{46}	ρ CH_3
41	832 m	832 (10)	826	819	30.00	2.97	34 S_{41} + 14 S_{45}	ν_{as} CCl_3
42	705 sh	705 sh	706	685	0.10	4.96	50 S_{42} + 18 S_{16} + 17 S_{17}	ρ CH_3
43	703 w	709 sh	703	685	3.42	4.80	53 S_{43} + 21 S_{23}	ν_{as} Si—C
44	668 sh	667 (16)	658	654	118.10	3.46	67 S_{41} + 24 S_{44} + 17 S_{46}	δ out-of-plane C=O
45	–	297 sh	288	285	1.01	0.61	12 S_{20} + 18 S_{25} + 17 S_{45}	δ_{as} CCl_3
46	–	216 (36)	207	208	0.13	1.00	50 S_{46} + 29 S_{47}	δ_{as} Si—C
47	–	214 sh	173	178	0.51	2.88	43 S_{47} + 19 S_{48} + 35 S_{49}	ρ Si—C
48	–	194 sh	160	151	0.14	3.09	11 S_{47} + 20 S_{48} + 60 S_{49}	ρ CCl_3
49	–	184 (50)	153	151	0.03	0.05	14 S_{50} + 20 S_{49} + 20 S_{51}	τ CH_3
50	–	184(50)	152	143	0.01	0.28	51 S_{31} + 51 S_{50}	τ CH_3
51	–	184 (50)	130	122	0.00	0.00	13 S_{30} + 39 S_{31} + 39 S_{51}	τ CH_3

Table 2 (*Continued*)

Mode	Infrared[a] (liquid)	Raman[a] (liquid)	Calculated[a]	Calculated SQM[b]	IR intensity[c]	Raman intensity[d]	Potential-energy distribution[e]	Approximate description of mode
52	–	–	68	–	0.91	0.08	–	τ Si—O
53	–	–	61	–	0.76	0.04	–	τ C—O
54	–	–	37	–	0.04	0.01	–	τ CCl_3
RMSD (cm^{-1})			62.44	8.92				

[a] B3LYP/6-311++G(d,p) calculation. Observed and calculated values in cm^{-1}. sh, shoulder; br, broad; s, strong; w, weak; m, medium; v, very.
[b] From scaled quantum mechanics force field (see text for further definition). Relative band heights in parentheses.
[c] Units are km mol^{-1}.
[d] Units are $Å^4$ $(amu)^{-1}$.
[e] Coordinate numbers correspond to Table S1 (supplementary material).

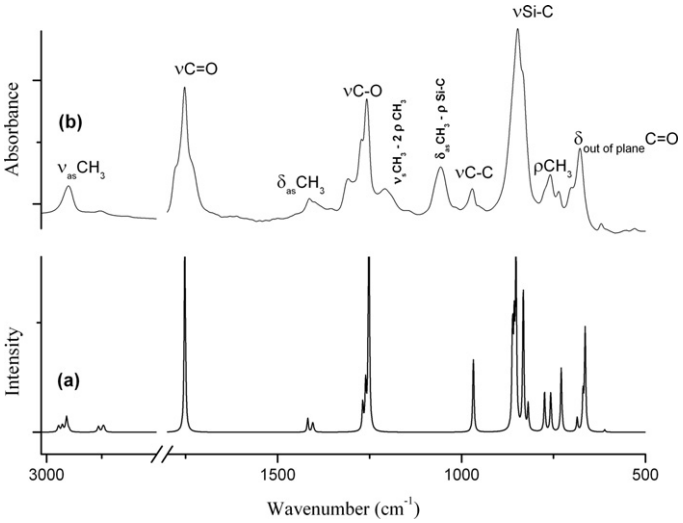

Fig. 3. Infrared spectra of $CCl_3C(O)OSi(CH_3)_3$. (a) The simulated (SQM) spectrum. (b) The liquid phase; resolution: 1 cm^{-1}.

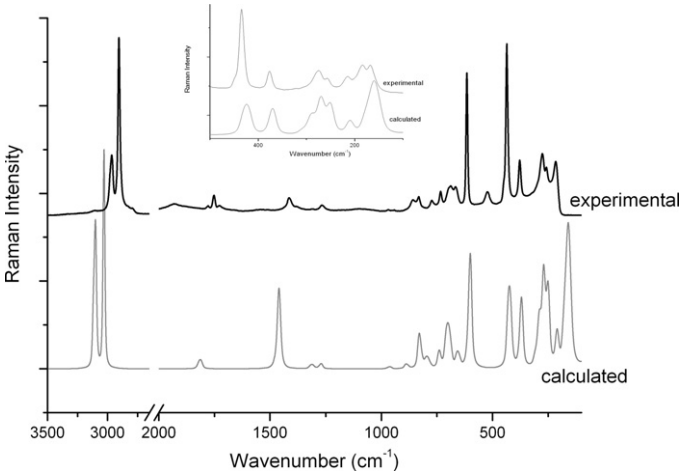

Fig. 5. Raman spectra of the liquid and simulated Raman spectra using Raman intensities according to the formula.

the liquid. The symmetric stretching mode of that group appeared as a very intense Raman band at 616 cm^{-1}; this band appeared at 626 cm^{-1} in the Raman spectrum of $CF_3C(O)OSi(CH_3)_3$ [14]. The $Si(CH_3)_3$ symmetric and two antisymmetric bending modes were observed at 275 and 258–216 cm^{-1} in the Raman spectrum. These modes appear to be strongly mixed with other vibrations in the normal vibrational modes of the molecule. To assign these bands correctly, the Raman polarized spectrum was used where the band at 275 cm^{-1} is strongly polarized (Table S1).

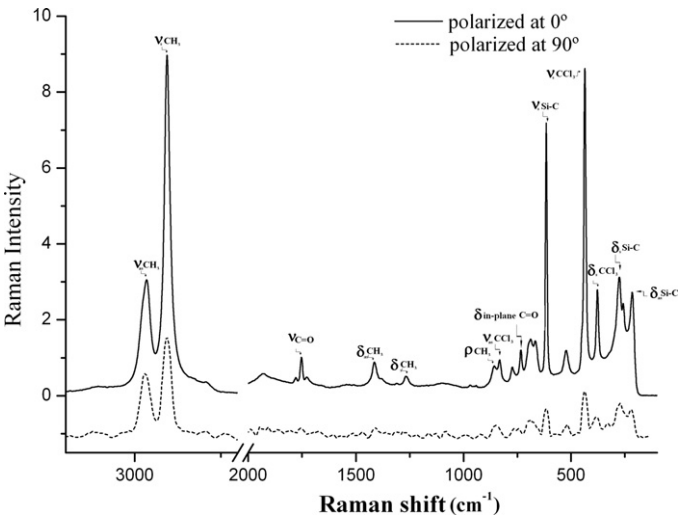

Fig. 4. Polarized Raman spectra of liquid $CCl_3C(O)OSi(CH_3)_3$ at room temperature (resolution: 4 cm^{-1}).

4.2.3. Carbonyl group modes

The very strong band observed at 1752 cm^{-1} in the liquid infrared spectrum was immediately assigned to the C=O stretching mode. The bands located at 735 and 668 cm^{-1} in the liquid spectrum were assigned to the CO in-plane and CO out-of-plane bending modes, respectively.

4.2.4. Trichloromethyl group modes

Two bands located at 832 and 436 cm^{-1} corresponds to the CCl_3 antisymmetric and symmetric stretching modes respectively. The corresponding assignments were made mainly by comparison with $CCl_3C(O)OR$ molecules [16,33] and with the calculations. On this basis, the very intense band located at 436 cm^{-1} was assigned to the CCl_3 symmetric stretching mode. In the Raman spectrum, the bands located at 377 was assigned to the symmetric deformation mode; 321 and 297 cm^{-1} were assigned to the CCl_3 antisymmetric deformation modes.

The CCl_3 rocking modes were assigned taking into account the predicted theoretical wavenumbers (Table 2). Thus, the bands located at 194 and 168 cm^{-1} in the Raman spectrum was assigned to the CCl_3 rocking modes.

4.2.5. Skeletal modes

The medium band at 970 cm^{-1} in the gas infrared spectrum was assigned to the $Cl_3C—CO$ stretching modes. This mode appeared in the 900 cm^{-1} region for the $CCl_3C(O)OR$ molecules reported previously [16,33]. In accordance with the predicted theoretical wavenumber, the band at 1259 cm^{-1} should be associated

primarily with OC—OSi. The assignment of the C(O)—O—Si bending vibration was difficult because of the large degree of mixing with other vibrations.

4.2.6. Torsional modes

Only a weak band located at 184 cm^{-1} in the Raman spectrum could be assigned to the CH_3 torsional modes.

4.3. Calculation of force constants

The force field in Cartesian coordinates, as generated by Gaussian, was transformed to the set of non-redundant natural coordinates defined in Table S2 and Fig. S1. Such coordinates take into account the local symmetry around the C and Si atoms and follow the proposals of Fogarasi et al. [34]. The resulting force field was subsequently scaled using the scheme proposed by Pulay et al. [35] and the initial scale factors were defined using unity for all modes [36], while the scale factor follows the proposals of Borowski et al. [37] with respect to the C—Cl bond, as shown in Table S3. These scale factors were subsequently refined by the nonlinear least-squares procedure in order to fit 54 experimental wavenumbers.

The refined scale factors corresponding to each force constant appear in Table S3, while the resulting wavenumbers, RMSD final value and the potential-energy distribution are given in Table 2. It can be seen that only one-half of the modes have a participation of ≥50% of the single coordinate, whereas other modes represent very complex vibrations where several coordinates are involved.

The SQM force field was used to calculate the internal force constants shown in Table S4 (supplementary material), where they are compared with the equivalent values for the previously studied trifluoroethyl trifluoroacetate. There is a decrease in the C=O stretching force constants when moving from $CF_3C(O)OSi(CH_3)_3$ to $CCl_3C(O)OSi(CH_3)_3$ with increasing f [C(1)—C(2)]. These differences are in accordance with the corresponding hyperconjugative interactions.

5. NBO results

The anomeric effect is well known in the case of interactions involving periplanar free electron pairs of oxygen atoms as in this case of substituent acetates with different sizes and electronegativity.

The observed interactions reported in Table S5 were obtained from NBO calculations for the anti form of the acetates substituted of the $CX_3C(O)O—R$ (X = F, Cl and R = CH_3, $Si(CH_3)_3$) form.

When R is more electropositive, there is an increase in the interaction of lone pairs (LP) from O to the σ^* C=O, with an increase in electron delocalization of the O—C=O group. The lone pairs of Cl and F atoms and their interaction on the σ^* C—C and σ^* C=O play an important role in the strength of these bonds.

Fig. 6 shows the interaction energy LP O → σ^* C=O of the $CCl_3C(O)OSi(CH_3)_3$ and related molecules function of the wavenumber C=O stretching mode (ν C=O).

We can see from this figure that the interaction of the lone pair of electrons from O to the antibonding orbital of the carbonyl group increases for the oxoacetates, while the wavenumber of the C=O bond decreases. This effect is greater when the C=O bond is attached to the CF_3 group than to the CCl_3 group. We may also note that the greater the difference in the electronegativity of the carbonyl bond environment, the more LP O → σ^* C=O interaction there is.

For a greater anomeric effect LPO → σ^* C=O, a shortening of the CO bond is expected. This is reflected in a value greater than the wavenumber of the CO bond stretching, as can be seen in Fig. 7, which illustrates the energy variation of the interaction LP O → σ^* C=O with respect to the wavenumber of the CO bond stretching (ν C—O).

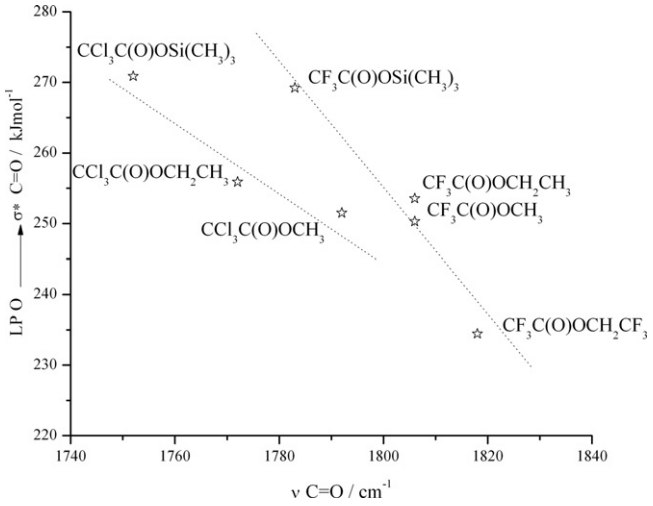

Fig. 6. Interaction energy LP O → σ^* C=O of the $CCl_3C(O)OSi(CH_3)_3$ and related molecules function of the wavenumber C=O stretching mode (ν C=O).

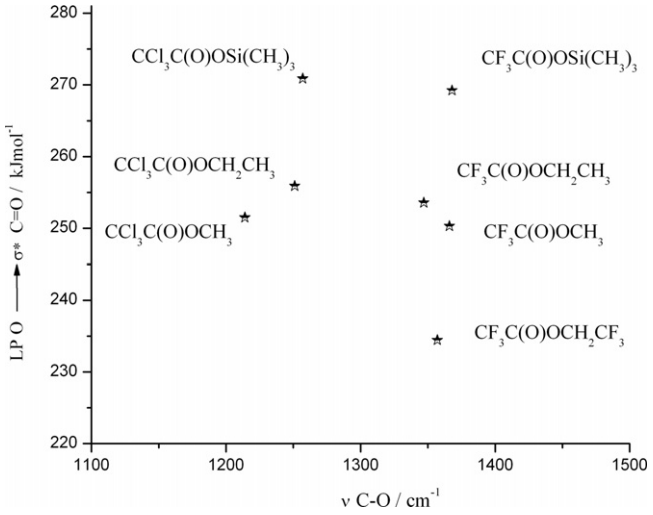

Fig. 7. Variation of interaction energy LP O → σ^* C=O function of ν C—O.

We may thus conclude that when the substituent is less electronegative, it favors the delocalization of the O—C=O group, strengthening the anion $CX_3C(O)O^-$. Hence, the molecule becomes more sensitive to nucleophilic attack.

6. AIM results

The quantum theory of atoms in molecules has repeatedly been useful in the characterization of bonds through a topological analysis of the electronic charge density and its Laplacian at the bond-critical point (BCP). In the AIM theory the nature of the bonding interaction can be determined through an analysis of the properties of the charge density, ρ, and its Laplacian $\nabla^2(\rho)$ at the BCP, and through the properties of the atom, which are obtained by integration of the charge density over the atomic basin. Table 3 presents the bond-critical point data for $CCl_3C(O)OSi(CH_3)_3$, $CF_3C(O)OSi(CH_3)_3$, $CCl_3C(O)OCH_3$ and $CF_3C(O)OCH_3$. As seen in Table 3, for these molecules the value of the charge density at the C—C bond-critical point is relatively high and $\nabla^2(\rho)$ is negative, indicating that the charge density has been concentrated in the internuclear region. In addition, the value of the charge density

Table 3
Calculated [RHF/6-311++G(d,p)] bond critical point (BCP) data, bond distances and wavenumbers.

	$CF_3C(O)OSi(CH_3)_3$	$CCl_3C(O)OSi(CH_3)_3$	$CCl_3C(O)OCH_3$	$CF_3C(O)OCH_3$
C—C				
ρ	0.2539	0.240	0.244	0.2543
$\nabla^2(\rho)$	−0.626	−0.538	−0.555	−0.629
λ_1/λ_3	1.272	1.183	1.189	1.275
q C1	0.992	−0.244	−0.354	0.992
q C2	0.734	0.782	0.664	0.725
ν	849 (849)	966 (950)	969 (882)	877 (869)
C—O				
ρ	0.3172	0.3186	0.3150	0.3153
$\nabla^2(\rho)$	−0.430	−0.446	−0.478	−0.464
λ_1/λ_3	0.888	0.901	0.955	0.935
q C2	0.734	0.782	0.901	0.725
q O	−0.808	−0.818	−0.348	−0.522
ν	1371 (1385)	1276 (1272)	1251 (1277)	1344 (1349)
C═O				
ρ	0.4221	0.4226	0.444	0.4248
$\nabla^2(\rho)$	−0.128	−0.131	−0.416	−0.086
λ_1/λ_3	0.655	0.653	0.642	0.644
q C2	0.734	0.782	0.901	0.725
q O	−0.555	−0.560	−0.633	−0.522
ν	1812 (1773)	1797 (1753)	1817 (1767)	1833 (1789)
O—Si/C				
ρ	0.195	0.1024	0.231	0.2271
$\nabla^2(\rho)$	0.566	0.577	−0.392	−0.247
λ_1/λ_3	0.205	0.206	0.979	0.976
q O	−0.808	−0.818	−0.348	−0.522
q Si/C	1.812	1.822	0.521	−0.215
ν	708 w	679	1021 s	1016 w

of the C—C bond in the fluorinated compounds is higher than in the chlorinated compound and $\nabla^2(\rho)$ is more negative. This behavior agrees with the polarity increase of the C—C bond. One can observe that the charge density decreases with the substitution of the Cl atom by F, which leads to an elongation in the C—C bond length. The covalent character of the C—C bond is only affected by the substituent change X (F, Cl) and there is a decrease in bond polarity when passing from the chlorinated to the fluorinated compounds. If we observe the behavior of the CO and C═O bonds, it may be seen that for the four molecules with large ρ and $\nabla^2(\rho) < 0$ values, typically covalent bonds are described. In the case of the methylated compound compared with the two silyl compounds, the $\nabla^2(\rho)$ value is more negative for the C—O than for the C═O bonds. The C═O bond charge density values ρ for $CF_3C(O)OCH_3$ are much higher than for the $CF_3C(O)OSi(CH_3)_3$ and $CCl_3C(O)OSi(CH_3)_3$ compounds. This agrees with the increased energy of interaction $LPO_{(C=O)} \rightarrow \sigma^*$ C—O, with the higher contraction of the C═O bond and with the lower polarity of the CO bond in the methylated than in Si compounds.

This behavior is reflected in the higher wavenumber vibration stretching modes of both methylated bonds in the molecule in comparison with the two silyl compounds. When changing the C by the Si atom, the oxygen atomic charge decreases markedly in the O—X bond while Si increases with a greater polarity in the Si—O bond, and a lower charge density and a Laplacian increase become evident.

7. Conclusions

Theoretical methods indicate two possible conformers, both with staggered $SiMe_3$ groups but with *anti* and *gauche* CCOSi dihedral angles, although the former is more stable by 36.9 kJ mol^{-1}. The most stable conformer has a C_s symmetry [dihedral angle ϕ(CCOSi) = 180°], where the $CC1_3$ group is staggered with respect to the $Si(CH_3)_3$ group. Using the experimental results of related molecules, and from the concept of conformational transferability, the most stable conformation was determined and the structure of $CCl_3C(O)OSi(CH_3)_3$ was predicted. Following this conceptual line, the conformational search was carried out based on the vibrational properties of the molecule. The results confirm that the anti-staggered conformation for $Cl_3C(O)OSi(CH_3)_3$ and related molecules is the most stable.

Infrared and Raman spectra were recorded for $CCl_3C(O)OSi(CH_3)_3$, and bands assignable to 52 of the expected 54 normal modes of vibration were observed. Only one conformer was detected in the liquid spectra. Using the observed wavenumbers it was possible to scale the theoretical force field. The resulting SQM force field served to calculate the potential-energy distribution that revealed the physical nature of the molecular vibrations and the force constants in internal coordinates, which were similar to the values obtained for related chemical species.

It is interesting to note how the rotation barrier is the same for the $CCl_3C(O)OSi(CH_3)_3$ and $CF_3C(O)OSi(CH_3)_3$ esters with respect to the COSiC dihedral angle in spite of the substituent change (F, Cl). This is reflected on the little displacements of the stretching bands of the modes corresponding to the CH_3 groups.

The NBO result indicates that when R is more electropositive there is an increase in the interaction of lone pairs (LP) from O to the σ^* C═O, with an increase in the O—C═O group electron delocalization. This behavior is reflected in the higher wavenumber stretching vibration modes of both methylated bonds in the molecule in comparison with the two silyl compounds.

Acknowledgments

We acknowledge research grants from CIUNT (Consejo de Investigaciones de la Universidad Nacional de Tucumán), CONICET (Consejo Nacional de Investigaciones Científicas y Técnicas, PIP 6457).

Appendix A. Supplementary data

Supplementary data associated with this article can be found, in the online version, at http://dx.doi.org/10.1016/j.vibspec.2012.11.014.

References

[1] J.M. Renga, P.C. Wang, Tetrahedron Lett. 26 (9) (1985) 1175–1178.
[2] E.G. Rochow, J. Am. Chem. Soc. 67 (1945) 963–965.
[3] E.G. Rochow, Chemistry of Silicones, Wiley, New York, 1951.
[4] A.D. Petrov, B.F. Mironov, V.A. Ponomarenko, E.A. Chernyshev, Synthesis of Organosilicon Monomers, Consultants Bureau, New York, 1964.
[5] K.M. Lewis, D.G. Rethwisch (Eds.), Catalyzed Direct Reactions of Silicon, Elsevier, Amsterdam, 1993.
[6] E.Y. Lukevitts, M.G. Voronkov, Organic Insertion Reactions of Group IV Elements, Consultants Bureau, New York, 1966.
[7] B. Marciniec (Ed.), Comprehensive Handbook of Hydrosilylation, Pergamon Press, New York, 1992 (references therein).
[8] Y.S. Song, B.R. Yoo, G.H. Lee, I.N. Jung, Organometallics 18 (1999) 3109–3115.
[9] E.W. Colvin, Silicon in Organic Synthesis, Butterworth, London, 1981.
[10] W.P. Weber, Silicon Reagents for Organic Synthesis, Springer-Verlag, New York, 1983.
[11] M.A. Brook, Silicon in Organic, Organometallic and Polymer, Wiley, New York, 2000.
[12] M.E. Defonsi Lestard, M.E. Tuttolomondo, E.L. Varetti, D.A. Wann, H.E. Robertson, D.W.H. Rankin, A. Ben Altabef, J. Mol. Struct. 917 (2009) 183–192.
[13] M.E. Defonsi Lestard, M.E. Tuttolomondo, E.L. Varetti, D.A. Wann, H.E. Robertson, D.W.H. Rankin, A. Ben Altabef, J. Raman Spectrosc. 40 (2009) 2053.
[14] M.E. Defonsi Lestard, M.E. Tuttolomondo, E.L. Varetti, D.A. Wann, H.E. Robertson, D.W.H. Rankin, A. Ben Altabef, J. Mol. Struct. 978 (2010) 114–123.
[15] M.E. Defonsi Lestard, M.E. Tuttolomondo, D.A. Wann, H.E. Robertson, D.W.H. Rankin, A. Ben Altabef, J. Raman Spectrosc. 41 (10) (2010) 1357.
[16] Y. Mido, K. Suzuki, N. Komatsu, M. Hashimoto, J. Mol. Struct. 144 (1986) 329–341.
[17] M.J. Frisch, G.W. Trucks, H.B. Schlegel, G.E. Scuseria, M.A. Robb, J.R. Cheeseman, J.A. Montgomery, Jr., T. Vreven, K.N. Kudin, J.C. Burant, J.M. Millam, S.S. Iyengar, J. Tomasi, V. Barone, B. Mennucci, M. Cossi, G. Scalmani, N. Rega, G.A. Petersson, H. Nakatsuji, M. Hada, M. Ehara, K. Toyota, R. Fukuda, J. Hasegawa, M. Ishida, T. Nakajima, Y. Honda, O. Kitao, H. Nakai, M. Klene, X. Li, J.E. Knox, H.P. Hratchian, J.B. Cross, C. Adamo, J. Jaramillo, R. Gomperts, R.E. Stratmann, O. Yazyev, A.J. Austin, R. Cammi, C. Pomelli, J.W. Ochterski, P.Y. Ayala, K. Morokuma, G.A. Voth, P. Salvador, J.J. Dannenberg, V.G. Zakrzewski, S. Dapprich, A.D. Daniels, M.C. Strain, O. Farkas, D.K. Malick, A.D. Rabuck, K. Raghavachari, J.B. Foresman, J.V. Ortiz, Q. Cui, A.G. Baboul, S. Clifford, J. Cioslowski, B.B. Stefanov, G. Liu, A. Liashenko, P. Piskorz, I. Komaromi, R.L. Martin, D.J. Fox, T. Keith, M.A. Al-Laham, C.Y. Peng, A. Nanayakkara, M. Challacombe, P.M.W. Gill, B. Johnson, W. Chen, M.W. Wong, C. Gonzalez, J.A. Pople, Gaussian 03, revision D.01, Gaussian, Inc., Wallingford, CT, 2004.
[18] C. Møller, M.S. Plesset, Phys. Rev. 46 (1934) 618.
[19] R. Krishnan, J.S. Binkley, R. Seeger, J.A. Pople, J. Chem. Phys. 72 (1980) 650.
[20] A.D. McLean, G.S. Chandler, J. Chem. Phys. 72 (1980) 5639.
[21] M.J. Frisch, J.A. Pople, J.S. Binkley, J. Chem. Phys. 80 (1984) 3265.
[22] W.J. Hehre, P.v.R. Schleyer, J.A. Pople, Ab Initio Molecular Orbital Theory, Wiley, New York, 1986.
[23] A.D. Becke, J. Chem. Phys. 98 (1993) 5648.
[24] C. Lee, W. Yang, R.G. Parr, Phys. Rev. B 37 (1988) 785.
[25] J.P. Perdew, K. Burke, M. Ernzerhof, Phys. Rev. Lett. 77 (1996) 3865 (Erratum: Phys. Rev. Lett. 78 (1997) 1396).
[26] E.D. Glendening, J.K. Badenhoop, A.D. Reed, J.E. Carpenter, F.F. Weinhold, Theoretical Chemistry Institute, University of Wisconsin, Madison, WI, 1996.
[27] R.F.W. Bader, H. Essen, J. Chem. Phys. 80 (1984) 5.
[28] R.F.W. Bader, Oxford Science Publications, Clarendon Press, London, 1990.
[29] W.B. Collier, Program FCARTP (QCPE #631), Department of Chemistry, Oral Roberts University, Tulsa, OK, 1992.
[30] B. Nielsen, A.J. Holder, GaussView, User's Reference, GAUSSIAN Inc., Pittsburgh, PA, 1997–1998.
[31] V. Krishnakumar, G. Keresztury, T. Sundius, R. Ramasamy, J. Mol. Struct. 702 (2004) 9.
[32] L.E. Fernández, A. Ben Altabef, E.L. Varetti, J. Mol. Struct. 553 (2000) 255.
[33] Y. Mido, T. Kawashita, K. Suzuki, J. Morcillo, M.V. Garcia, J. Mol. Struct. 162 (1987) 169–182.
[34] G. Fogarasi, X. Zhou, P.W. Taylor, P. Pulay, J. Am. Chem. Soc. 114 (1992) 8191.
[35] P. Pulay, G. Fogarasi, G. Pongor, J.E. Boggs, A. Vargha, J. Am. Chem. Soc. 105 (1983) 7037.
[36] F. Kalincsák, G. Pongor, Spectrochim. Acta A 58 (2002) 999.
[37] P. Borowski, A. Drzewiecka, M. Fernández-Gómez, M.P. Fernández-Liencres, T. Peña Ruiz, Vib. Spectrosc. 52 (2010) 16–21.